*energies*

MDPI

*Article*

# Design and Development of High-Power, High-Efficiency, and Low-Noise Microwave Sources for Wireless Power Transmission

**Kaviya Aranganadin and Ming-Chieh Lin ***

Multidisciplinary Computational Laboratory, Department of Electrical and Biomedical Engineering, Hanyang University, Seoul 04763, Republic of Korea; kavihanyang@gmail.com
* Correspondence: mclin@hanyang.ac.kr

**Abstract**

This study investigates the feasibility and possible improvement of microwave power transmission (MPT) in a space-based solar power system (SSPS). SSPS, a concept proposed by Dr. Peter Glaser in 1968, aims to harness solar energy in space, free from atmospheric constraints, and transmit it to Earth using microwaves or lasers. Our focus is on enhancing the efficiency and cost-effectiveness of MPT, which accounts for a significant portion of SSPS expenses. In this work, we propose the use of a novel field emission-based rising-sun magnetron (RM) in the MPT subsystem, aiming to extend system longevity and simplify construction, while dramatically reducing the implementation cost. It is demonstrated that the optimization of the RM design at 2.45 GHz can achieve a high output power of >100 kW with a high efficiency of >85%, based on the well-established conformal finite-difference time-domain particle-in-cell simulations. This research provides valuable insights into improving SSPS, making it a more viable and sustainable renewable energy solution.

**Keywords:** Field emission; microwave; rising-sun magnetron; solar based energy technology; wireless power transmission

check for updates

Academic Editor: William Holderbaum

Received: 30 August 2025
Revised: 26 September 2025
Accepted: 13 October 2025
Published: 16 October 2025

**Citation:** Aranganadin, K.; Lin, M.-C. Design and Development of High-Power, High-Efficiency, and Low-Noise Microwave Sources for Wireless Power Transmission. *Energies* **2025**, *18*, 5451. https://doi.org/10.3390/en18205451

**Copyright:** © 2025 by the authors. Licensee MDPI, Basel, Switzerland. This article is an open access article distributed under the terms and conditions of the Creative Commons Attribution (CC BY) license (https://creativecommons.org/licenses/by/4.0/).

## 1. Introduction

Space-based solar power is the concept of collecting solar energy in orbit and transmitting it to Earth [1]. Unlike ground-based solar collectors, it offers longer operating periods, minimal atmospheric interference, and orbital positioning that enables nearly continuous energy capture. A considerable fraction, about 55–60%, of incident solar energy fails to reach the surface of the Earth due to atmospheric reflection, absorption, and scattering. A space-based solar power system (SPSS) converts sunlight into microwaves or lasers beyond the atmosphere, thereby eliminating atmospheric losses and rotational downtime, though at the significant expense of orbital deployment. Space-based solar power is regarded as a form of sustainable or renewable energy and an environmentally friendly option. It might be one of the best candidates to solve all the problems of fossil fuel depletion, nuclear waste production, and global warming at once. The concept of an SSPS, originally known as a satellite solar-power system, was first proposed by Dr. Peter Glaser in November 1968 [2], and the technique of transmitting power from an SSPS to the surface of Earth by directing microwaves from a large satellite antenna to a ground-based rectenna was patented in 1973 [3]. The National Aeronautics and Space Administration (NASA) granted contract [4] highlighted major obstacles, notably the expense of transporting materials into orbit and the lack of large-scale space project experience, but determined that the concept was promising enough to justify further research. Between 1978 and 1986, the United States

Congress authorized the NASA and the Department of Energy (DoE) to conduct a joint study of the concept, leading to the Satellite Power System Concept Development and Evaluation Program [5,6]. The study remains the most extensive to date, with a budget of 50 million USD [7]. Several reports were produced assessing its engineering feasibility, and one of them, entitled "Power Transmission and Reception Technical Summary and Assessment," was related to the wireless power transmission (WPT) [8], which is the most important sub-system of SSPS. The project was discontinued for several decades following the change in administrations after the 1980 US federal elections. NASA renewed its assessment of SSPS feasibility in 1997, taking into account the technological progress of the period and asserted that the "US National Space Policy now calls for NASA to make significant investments in technology (not a particular vehicle) to drive the costs of Earth to Orbit (ETO) transportation down dramatically. This is, of course, an absolute requirement of space solar power" [9]. NASA established the Space Solar Power Exploratory Research and Technology program (SERT) in 1999 to investigate solar power satellite (SPS) architectures. The program explored concepts for a gigawatt-level space power system capable of converting sunlight into electricity and transmitting it to Earth, and it identified a pathway for advancement using the current technologies available during that time. As part of its studies, SERT proposed inflatable gossamer structures with photovoltaic arrays and concentrator lenses or solar heat engines for power generation. It assessed both sun-synchronous and geosynchronous orbits, estimating that SPS would only be economically viable if launch costs were in the range of USD 100–USD 200 per kilogram of payload to low Earth orbit [7]. In 2009, Dr. Pete Worden argued that space-based solar power was approximately five orders of magnitude more costly than solar power generated in the Arizona desert, with transportation of materials to orbit being the primary expense. He further described potential solutions as speculative and unlikely to be available for several decades at the earliest [10]. In recent decades, SSPS has been actively pursued by Japan, China, and Russia. In 2008, Japan enacted the Basic Space Law, designating space solar power as a national objective [11], and the Japan Aerospace Exploration Agency (JAXA) subsequently prepared a roadmap toward its commercialization. On 2 November 2012, China proposed a space cooperation initiative with India that included SSPS [12]. In 2015, the China Academy of Space Technology (CAST) presented its roadmap at the International Space Development Conference (ISDC), outlining a plan for a 1 GW commercial system by 2050 and releasing both a video [13] and a description [14] of their design. On 12 March 2015, JAXA reported the successful wireless transfer of 1.8 kW over a distance of 50 m to a small receiver by converting electricity into microwaves and then reconverting it back into electricity [15,16]. In the same year, Mitsubishi Heavy Industries demonstrated a 10 kW transmission to a receiver located 500 m away [17]. The WPT technology aims to replace conventional cable-based transmission of electricity, and recent successful demonstrations suggest broad potential for terrestrial applications [18]. However, ongoing research in WPT highlights several technical challenges, such as beam divergence over long distances, alignment and tracking accuracy, rectenna conversion losses, and the limited lifetime of conventional microwave sources [8]. Researchers have explored a range of approaches, including microwave-based WPT using solid-state phased arrays and klystrons for beam-forming and frequency stability, as well as laser-based optical power transmission for higher precision [14,18]. While solid-state systems offer excellent control and scalability, they are often limited by lower efficiency and high cost per watt. Laser-based systems provide better directional control but suffer from atmospheric attenuation and require a strict line of sight [18]. In contrast, microwave-based WPT using magnetrons provides high efficiency and simpler hardware, but with trade-offs in beam control and long-term source reliability [8]. Solving these challenges is essential for realizing reliable and efficient

wireless energy transfer over long distances, which will facilitate the transmission of power to locations where the installation of power cables has been difficult or dangerous. The SSPS/WPT systems are expected to enable power transmission for diverse applications, with one of the most immediate possibilities being wireless charging of electric vehicles. The WPT approach under development for SSPS relies on microwave technology, which, once matured, will allow power delivery across distances far greater than any existing system [18]. In this concept, electricity is generated by solar cell panels aboard a geostationary satellite positioned 36,000 km above Earth. The harvested energy is transmitted to the surface via microwave or laser links without cables, and subsequently converted into usable electrical power. Because the source is renewable and environmentally clean, the SSPS is anticipated to play a major role in addressing global energy demand while also contributing to environmental sustainability.

Table 1 lists the key parameters of the microwave power transmission used in a 1 GW commercial SSPS proposed by CAST, China [14], where 128,000 units of 5.8 GHz conventional magnetrons (CMs) at a power level of 12.5 kW with ∼54% of efficiency are required, and a mass of 4000 Tons is estimated. The corresponding cost of this subsystem can be found in Table 2. As one can see, the cost of the microwave power transmission is about USD 9210M, consisting of ∼30% of the total cost of the SSPS. The main portion of the high cost is due to the development and transportation requirements associated with the large number and mass of magnetrons in the subsystem. As the WPT is the most important sub-system of an SSPS and the current rates on the Space Shuttle run between USD 7000 and USD 11,000 per kilogram of transported material, this becomes one of the main hurdles against the realization of an SSPS [18].

**Table 1.** Summary of primary parameters of the MPT for a 1 GW Multi-Rotary Joints SPS (MR-SPS) [14].

| | | |
|---|---|---|
| Microwave power transmission | Frequency of microwave | 5.8 GHz |
| | Efficiency | ∼54% |
| | Diameter of transmitting antenna | 1000 m |
| | Number of antenna modules | 128,000 |
| | Transmitting power of an antenna module | 12.5 kW |
| | Mass | 4000 t |
| | Diameter of receiving antenna | 5 km |

**Table 2.** The cost analysis result of space segment (million USD) [14].

| Sub-System | Design | Development | Transportation (1000 USD/kg) | Construction | Operation and Maintenance | Close and Recycle | Total |
|---|---|---|---|---|---|---|---|
| SECC | 5 | 2000 | 2000 | 1200 | 200 | 200 | 5605 |
| PTM | 5 | 2000 | 2500 | 1000 | 500 | 250 | 6255 |
| MPT | 10 | 3600 | 4000 | 800 | 400 | 400 | 9210 |
| Structure | 5 | 600 | 1200 | 550 | 50 | 120 | 2525 |
| AOC | 5 | 500 | 100 | 200 | 2500 | 10 | 3315 |
| TM | 5 | 150 | 150 | 0 | 150 | 15 | 470 |
| ISRM | 10 | 250 | 50 | 100 | 250 | 5 | 665 |
| Total | 45 | 9100 | 10,000 | 3850 | 4050 | 1000 | 28,045 |

The MPT subsystem is pivotal in SSPS, requiring robust and efficient microwave generation technology. Here, the cavity magnetron, widely used in applications like radars and microwave ovens, emerges as a critical component. Characterized as a high-efficiency, high-power, and low-cost device, the magnetron produces microwave oscillations

through electron interaction in crossed electric and magnetic fields with metal cavity resonators [19–27]. Despite its efficiency, typically around 66.7% in commercial applications, and potential to reach above 90%, the lifespan of traditional magnetrons is limited mainly due to cathode degradation [22]. The cavity magnetrons generally employ a thermionic or heated cathode [24], which is biased at a high negative potential by a high-voltage direct-current power supply, while the anode is held at ground potential. The cathode filament is typically composed of tungsten with a small addition of thorium to enhance electron emission [25]. Although thorium is a radioactive element, the associated cancer risk is negligible under normal operating conditions, since it does not become airborne. A potential hazard arises only if the filament is removed from the magnetron, ground into fine particles, and inhaled. Nevertheless, the operational lifetime of a magnetron is primarily constrained by the thermionic cathode, which is often shortened by surface contamination, a phenomenon referred to as cathode poisoning. Under such conditions, the emissive coating degrades rapidly when subjected to excessive current loading, resulting in reduced electron emission and diminished output power. Recently, field emission arrays have demonstrated current densities exceeding 100 $A/cm^2$ [28], suggesting the feasibility of employing field emission electron sources, or cold cathodes, in microwave tubes. Addressing this, our work proposes the use of field emission-based magnetrons in SSPS MPT.

This innovation can extend the lifespan, simplify assembly, and reduce costs, making SSPS more viable. The "rising sun" configuration of these magnetrons further eases fabrication and enhances reliability [24–35]. Our approach integrates state-of-the-art conformal finite-difference time-domain (CFDTD) particle-in-cell (PIC) simulation [20–27] to optimize this design for SSPS applications. Replacing a thermionic cathode with a field emission cathode can both extend device lifetime and significantly reduce the complexity of the external circuitry and assembly process. By advancing magnetron technology, we aim to overcome one of the key hurdles in SSPS, thereby contributing to the development of a sustainable and efficient space-based solar power generation system.

The remainder of this article is organized as follows: Section 2 provides a detailed description of the simulation models and setup. Section 3 presents the simulation results and provides a comprehensive discussion. Finally, Section 4 summarizes the main conclusions of this study.

## 2. Simulation Models and Setup

The design and optimization of the rising-sun magnetron (RM) have been carried out using the CFDTD PIC simulation as implemented in VSim. This advanced simulation technique is beneficial for several reasons, such as accuracy in complex geometries by the implementation of the Dey–Mittra cut-cell boundary algorithm, allowing for the accurate modeling of curved boundaries within the VORPAL framework [29,30], speed and efficiency, robustness to material boundaries, and improved emission algorithms. The design parameters of the magnetron have been verified to operate at the targeted 2.45 GHz frequency, confirmed through a CFDTD simulation with a grid resolution of $102 \times 102$ and corroborated by finite element method (FEM) frequency domain calculations with over 99% accuracy [23,36]. The dispersion curve of a magnetron is a crucial characteristic that indicates the relationship between the frequencies of the modes of oscillation and their phase shifts. Adequate mode separation on the dispersion curve is essential for the stable operation of a magnetron, as it helps to ensure that the desired mode of oscillation can be maintained without interference from adjacent modes. In a CM, mode separation can be difficult to achieve due to the symmetrical nature of the side cavities, often requiring additional components like straps to achieve the desired separation. The RM configuration presents a significant advantage over conventional designs by inherently providing better

mode separation. The asymmetric structure of the rising-sun design allows for the natural suppression of undesired modes, which helps to ensure that the π mode can be isolated and stabilized. This intrinsic property of the RM not only simplifies the design by eliminating the need for straps but also reduces the risk of mode jumping and mode competition, which can lead to inefficiencies and unstable operation, as illustrated in Figures 1 and 2.

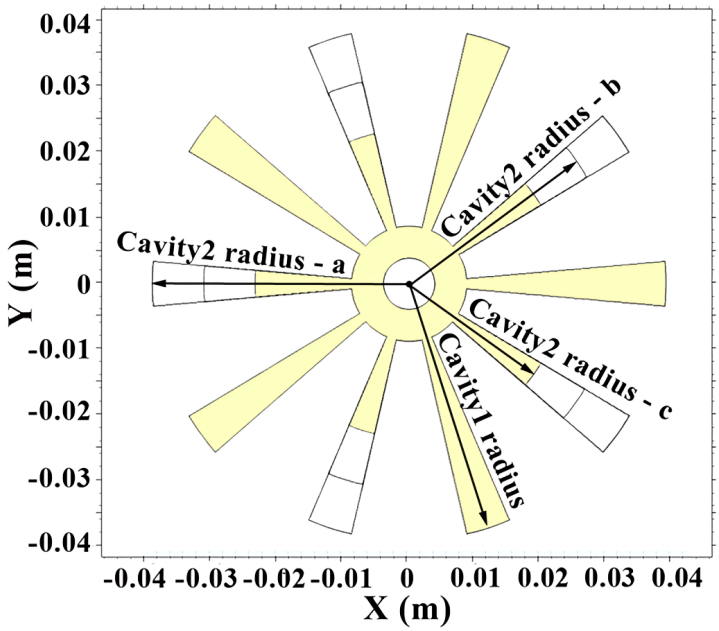



**Figure 1.** Scaling of the geometry parameters from a conventional magnetron (CM), case a, to a 2.45 GHz rising-sun magnetron (RM), case c.

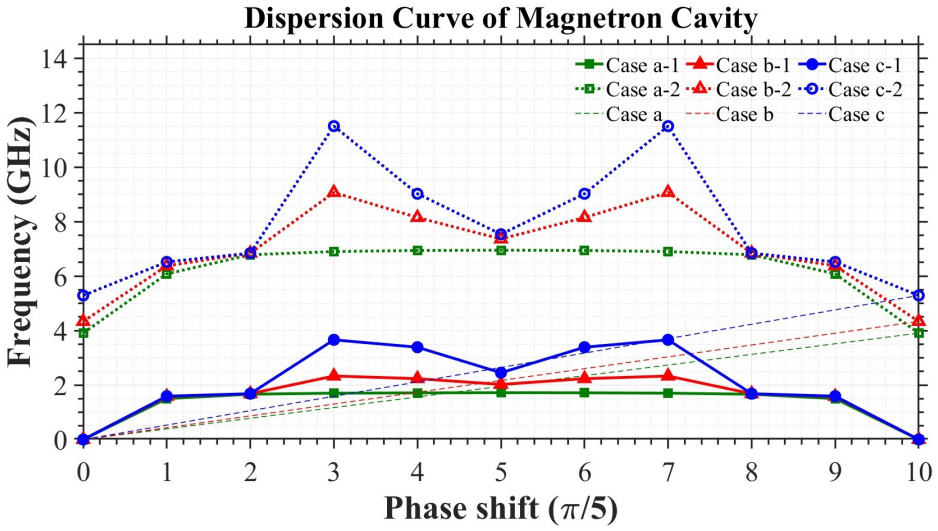



**Figure 2.** Dispersion curves of CM and RM cavities.

To investigate the effect of cavity geometry on mode separation, three design cases were analyzed with varying cavity radii, as illustrated in Figure 1. In case a, both cavity1 and cavity2 have a radius of 3.89 cm, leading to insufficient mode separation. Case b modifies the cavity2 radius to 3.11 cm, achieving greater mode separation for the π mode, as evidenced by the dispersion curves. Case c further reduces the radius of cavity2 to 2.334 cm, attaining the desired frequency of 2.45 GHz for the π mode with significant mode separation from adjacent modes of the 3π/5 and 4π/5 modes, which exhibit pretty large frequency shifts. Figure 2 shows the corresponding dispersion relations for the three geometries, featuring two eigenfrequency branches versus phase shift.

Figure 3 explores the π-mode frequencies as a function of the RM normalized geometric parameters, optimized at 2.45 GHz. This normalization facilitates geometry optimization, correlating with the practical dimensions of the magnetron, specifically an anode radius of 0.872 cm, a cavity1 radius of 3.89 cm, and angles of 0.174 radians for both cavity1 and cavity2. The corresponding Hull cutoff and Buneman–Hartree (B–H) curves of CM (case a) and RM (case c) cavities are shown in Figure 4. The schematic of a 10-vane field emission-based RM, designed using the VSim code, is shown in Figure 5. It details the geometry parameters and radio frequency (RF) output loading, with the design aimed at fostering π-mode oscillation. During stable, resonant operation, we anticipate the formation of five electron cloud spokes, indicative of the desired mode. Optimized geometric parameters, essential for determining the operational frequency of the cavity, are provided in Table 3. Finally, Figure 6 presents the dispersion curves for the RM, computed and verified through cold test simulations using both the FEM and CFDTD methods alongside a hot test simulation employing the CFDTD PIC technique. The π-mode interception with the operating curve is cleanly achieved, with minimal mode competition. However, attention must be given to the π/5 mode at 1.59 GHz, which, due to its proximity to the operating curve, could potentially compete with the π mode.

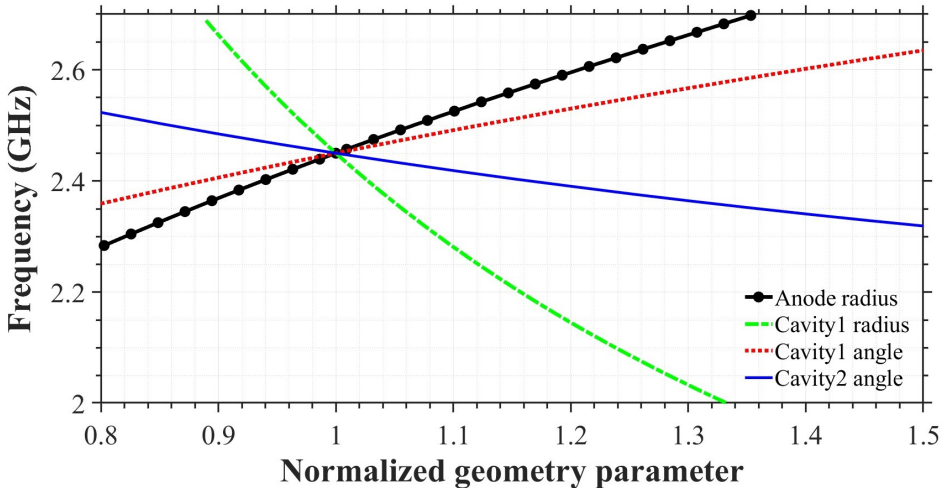



**Figure 3.** Relationship between π-mode frequency and normalized cavity geometry parameters of the RM model using the finite element method.

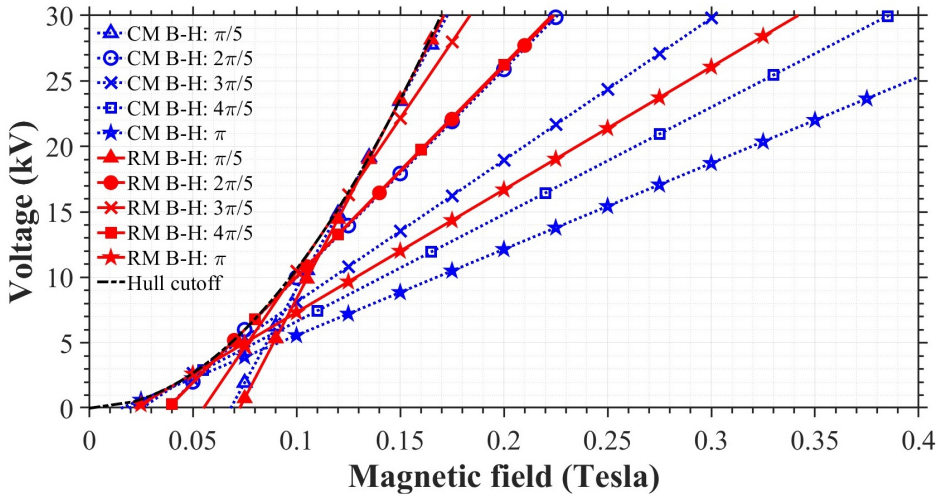



**Figure 4.** Hull cutoff and Buneman–Hartree characteristics of the CM (case a) and RM (case c) models for the π/5, 2π/5, 3π/5, 4π/5, and π modes.

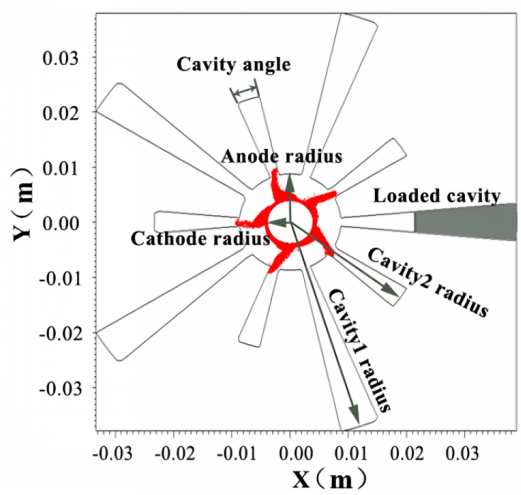



**Figure 5.** Schematic of a 10-vane field emission-based RM illustrating the key geometric parameters and an RF output load used in the VSim CFDTD PIC simulation.

**Table 3.** RM dimensions in the CFDTD PIC simulation.

| Cavity Geometry Parameters | Dimensions |
|---|---|
| Cathode radius | 0.389 cm |
| Anode radius | 0.872 cm |
| Cavity1 radius | 3.890 cm |
| Cavity2 radius | 2.334 cm |
| Cavity angle | 10.0 degree |

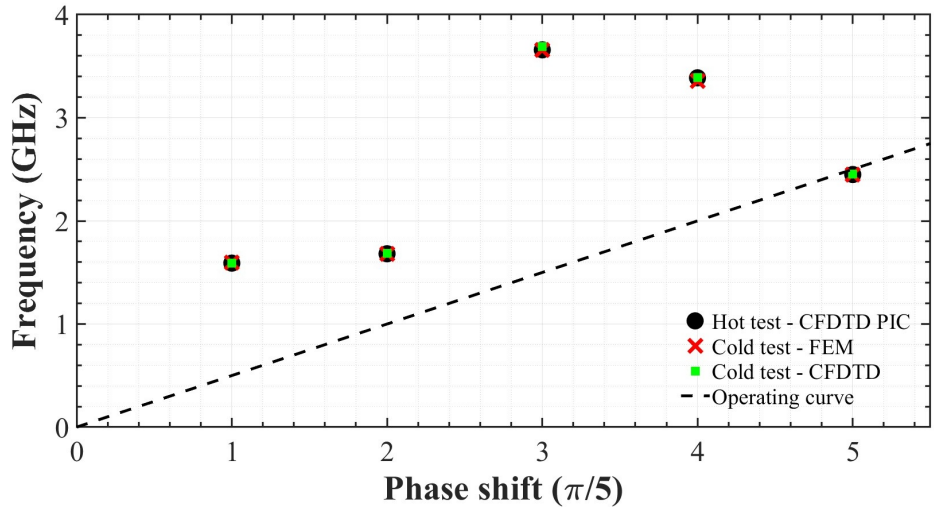



**Figure 6.** Benchmark of the rising-sun magnetron using the cold test simulations with the FEM and CFDTD method, and a hot test simulation with the CFDTD PIC method.

In the simulation, to approximate the RF power output and dissipation in the magnetron, a single long cavity along the horizontal x-axis is loaded with an absorber. This setup emulates the power coupling and acts as a control for the loaded quality factor (Q), which is set at 336 in this instance. Although a true output port is absent in the 2D simulation, we can simulate the power output by directing the port toward the absorber, enabling us to estimate the magnetron efficiency. The CFDTD scheme, particularly when coupled with PIC simulations, can mimic the real-world operating conditions of the magnetron, including thermal effects and electron emission characteristics. This comprehensive approach

ensures that the simulations are not just theoretical but also have practical applicability, forecasting how the magnetron will perform under actual operational stresses.

## 3. Simulation Results and Discussion

In our comprehensive simulation study using the CFDTD PIC methodology, the emission of macro-particles was carefully regulated at 50 particles per cell for each time step. The simulations were conducted within a 102 × 102 cell resolution grid, covering an 8.2 cm square domain, to ensure detailed spatial analysis. The total time duration of these simulations was extended to 1000 ns, a timeframe established post extensive convergence testing to ensure the accuracy of the results.

The operation of the RM is meticulously optimized by adjusting critical parameters such as the cathode–anode voltage ($V_{ca}$) and the applied magnetic field (B). This optimization process can be visualized on an efficiency (B-V) map, intersected by the Hull cutoff and the Buneman–Hartree (B-H) resonance conditions, as depicted in Figure 7. The simulations underscore the delicate balance required for stable magnetron oscillation: excessively high voltages at a fixed magnetic field disrupt stability, while insufficient voltages lead to suboptimal efficiency, in alignment with the B-H theory [31,32]. Furthermore, the simulations reveal that voltages near but below the Hull cutoff can induce mode competition, often manifesting as oscillation between the desired π mode at 2.45 GHz and the competing π/5 mode at 1.59 GHz. When faced with severe mode competition, the electron spokes exhibit instability, detracting from the device performance. To resolve these challenges, numerous simulation iterations have been conducted to pinpoint an optimal operating point that maximizes both the output power and efficiency of the RM. The culmination of these efforts is illustrated in Figure 7, where a distinct operational region has been identified. At this juncture, marked by a red star, the magnetron achieves an impressive efficiency of 85.4%. This point lies strategically above the Hartree resonance line and below the Hull cutoff voltage, indicating a harmonious balance between voltage and magnetic field strength conducive to high-efficiency, stable π-mode operation without being affected by mode competition. These results not only validate the theoretical underpinnings of magnetron operation but also pave the way for the practical realization of high-efficiency microwave sources. The RM, with its optimized design and operational parameters, stands poised to enhance the performance of SSPS/MPT systems and other high-power applications where efficiency and stability are paramount.

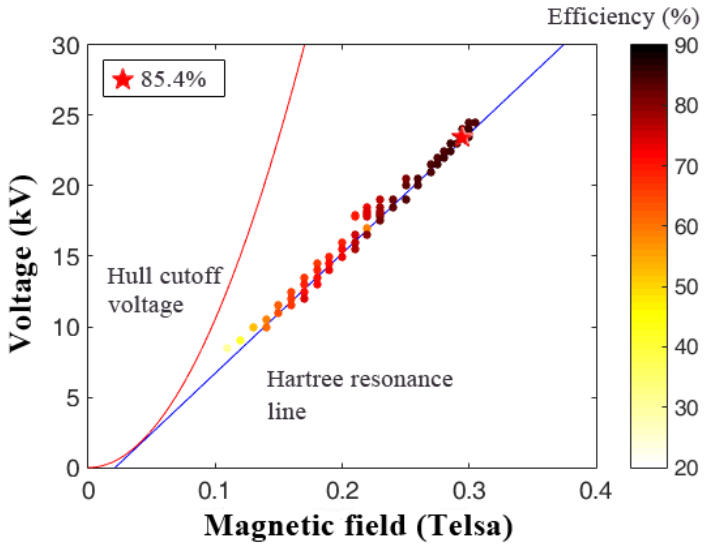



**Figure 7.** Operating conditions of the 2.45 GHz RM model represented in an efficiency (B-V) map with the corresponding Hull cutoff and Buneman–Hartree resonance curves.

Figure 8a presents the spectral analysis of the oscillations within cavity1, extracted from a 1000 ns CFDTD PIC simulation. The Fast Fourier Transform (FFT) reveals a dominant π-mode oscillation at 2.45 GHz, under an applied voltage of 23.5 kV and a magnetic field strength of 0.295 T. This frequency signature confirms the robustness of the π mode under the given simulation conditions. Complementing this spectral view, Figure 8b illustrates the temporal stability of the loaded cavity voltage over time. The plot highlights the "start-up" phase, where the oscillation frequency stabilizes, signifying the transition to a steady-state operation. During this phase, the growth in anode current and cavity power is indicative of the magnetron transition from initiation to stable operation. Through this diagnosis, the start-up time for the magnetron has been identified at approximately 90 ns.

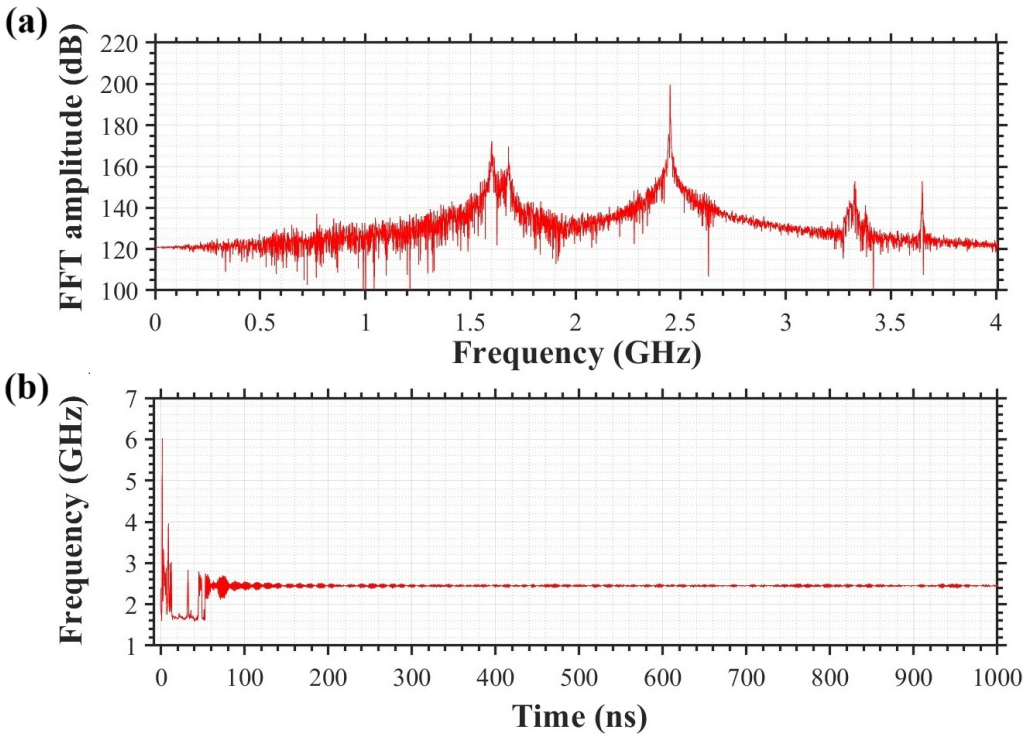



**Figure 8.** (**a**) FFT of the cavity1 voltage of the field-emission-based rising-sun magnetron over the entire simulation time and (**b**) time evolution of the resonant frequency, indicating a start-up time of 90 ns, from the CFDTD PIC simulation.

The dynamic evolution of the electron spoke formation is captured in Figure 9, showcasing the sequential development of the π-mode pattern. By 144 ns, the electrons are bunched into a well-defined π-mode configuration, demonstrating the swift establishment of the desired operating mode. This visual documentation of the electron spoke progression is instrumental in verifying the start-up period and the subsequent stabilization of the magnetron π-mode oscillation. These figures collectively serve as critical diagnostic tools in evaluating the performance and operational efficiency of the magnetron. Through both spectral and temporal analyses, coupled with direct visual inspection of electron dynamics, we gain comprehensive insights into the magnetron behavior from ignition to the steady-state phase. This multi-faceted approach is essential for confirming the theoretical predictions and ensuring the practical viability of the RM design. In this design, one of the large cavities of the RM was loaded with an absorber along the x-axis to model the output coupling and the RF dissipation. The absorber is parameterized as a cavity load whose loss is tuned to set the magnetron loaded Q, which is 336 in this configuration. For the 2D simulation, there is no genuine output port for this model, but it is feasible to mimic the device output using the port leading to the absorber and the corresponding power density to calculate the efficiency of this magnetron.

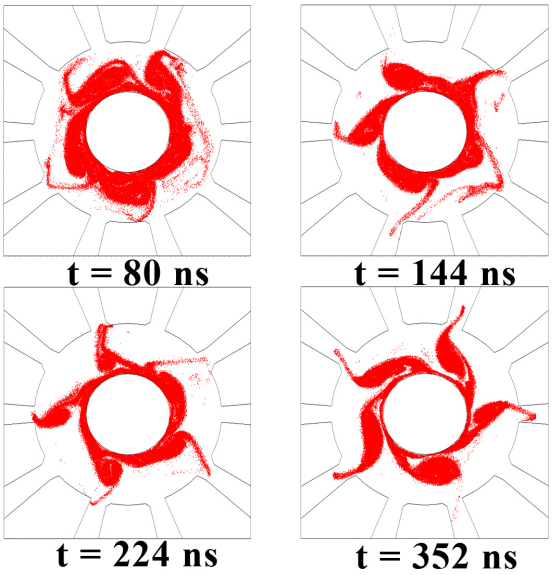



**Figure 9.** Screenshots of electron clouds at 80 ns, 144 ns, 224 ns, and 352 ns from the 2D CFDTD PIC simulations of the rising-sun magnetron at $V_{ca}$ = 23.5 kV and B = 0.295 T. The red dots represent electron macroparticles. At 144 ns, the electrons are bunched into a well-defined $\pi$-mode configuration.

Figure 10a shows the simulation results of the averaged cathode–anode voltage and anode current represented by a red solid line and a blue dotted line, respectively. The average procedure was done with a low-pass filter analyzer provided in the analyze window for post-processing in the VSim code. The linear anode current density is determined by averaging the anode current after oscillation, which is stable at about 212.1 A/m. The product of the cathode voltage and the averaged anode current density gives the linear input power density of about 4.985 MW/m. The averaged linear output power from the 2D CFDTD PIC simulation is about 4.255 MW/m, as shown in Figure 10b, so the output efficiency is determined to be 85.4%.

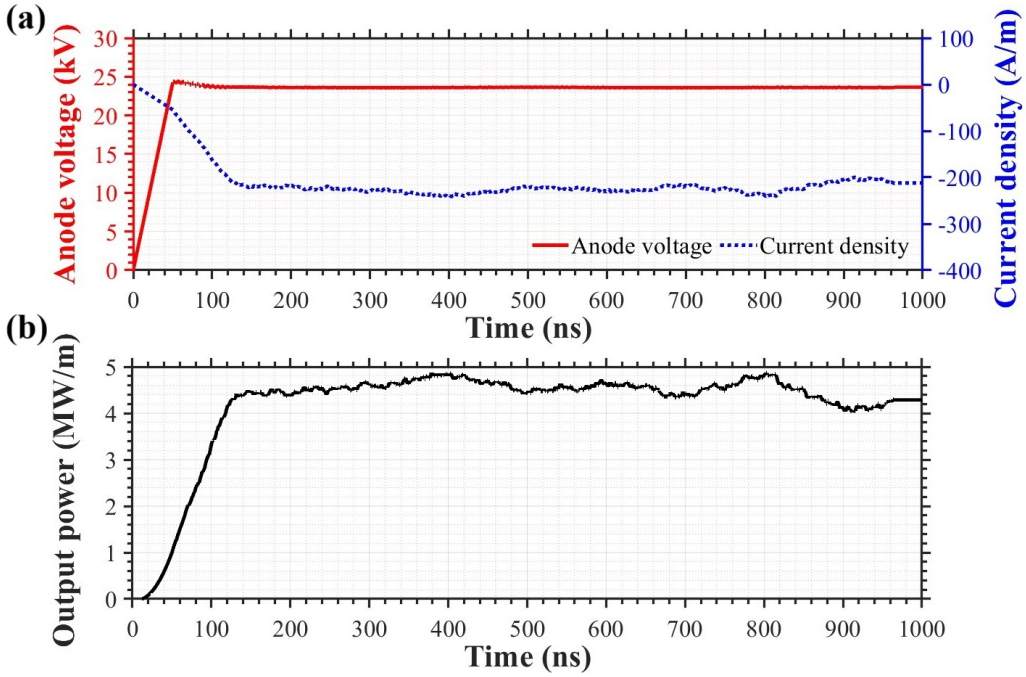



**Figure 10.** (**a**) Anode voltage and averaged anode linear current density, and (**b**) averaged output loading power evaluated using the CFDTD PIC simulation at the applied voltage $V_{ca}$ = 23.5 kV and static magnetic field B = 0.295 T.

The output power distribution across a range of magnetic field and voltage values simulated is illustrated as an output power (B-V) map in Figure 11. The red star denotes the high-efficiency operating point of 85.4% with a corresponding output power of 4.255 MW/m, obtained from the 2D CFDTD PIC simulation. This output power map serves as a useful reference for identifying favorable operating conditions for rising-sun magnetrons, helping to distinguish regions of high output power with lower efficiency, which are less suitable for practical implementation. Figure 12 shows the output power and efficiency of commercially available 2.45 GHz CMs. Extrapolating from the 2D simulations to a potential 3D design, assuming an RM with a cavity height of 2.5 cm, maintains the same cross-sectional profile as observed in the x-y plane. This model predicts a current density of approximately 0.869 A/cm$^2$, a value within the capabilities of field emission arrays or cold cathodes under the maximally achievable current density demonstrated experimentally [28]. The extrapolated output power for such a design stands at an estimated 106.4 kW, affirming the potential of this design for application in the proposed WPT subsystem.

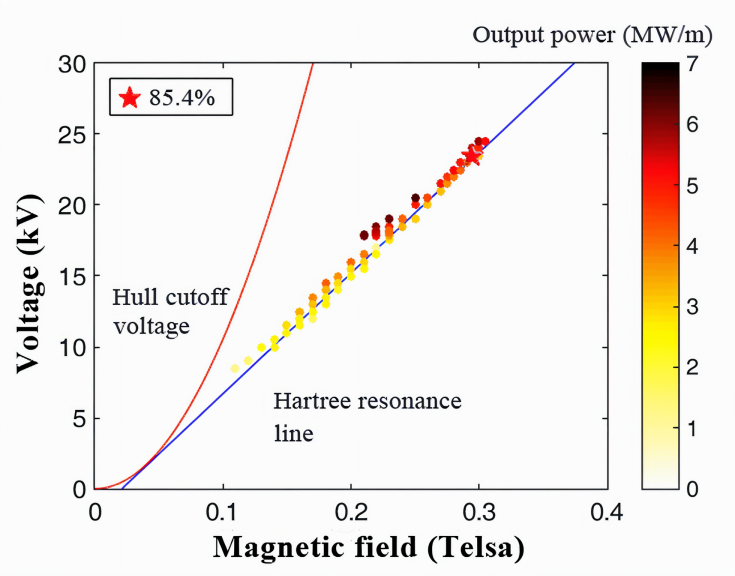



**Figure 11.** Operating conditions of the 2.45 GHz RM model represented in an output power (B-V) map with the corresponding Hull cutoff and Buneman–Hartree resonance curves.

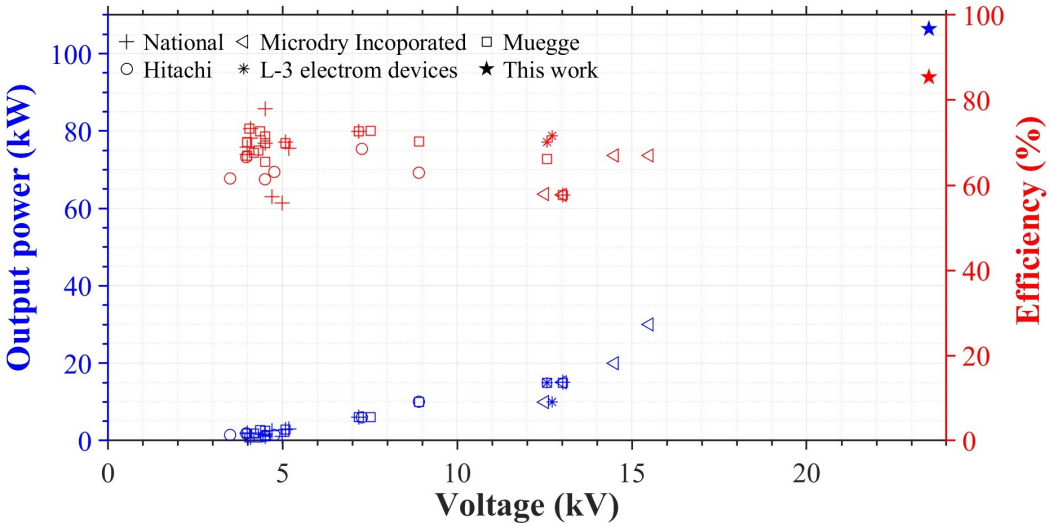



**Figure 12.** Output power and efficiency of commercially available magnetrons at 2.45 GHz. The solid star shows the best result of this work at 23.5 kV with an output power of 106.4 kW at a 85.4% efficiency.

## 4. Conclusions

From the hot test simulation results based on the well-established CFDTD PIC modeling, it has been demonstrated that a preliminary 2.45 GHz RM design after the optimization would achieve a high output power of >100 kW with a high efficiency of >85% using a feasible field emission current according to the achievable current density from widely available FEAs. Compared with a conventional strapped magnetron with a thermionic cathode, the proposed field-emission based rising-sun magnetron simplifies fabrication and assembly by eliminating the heater and strapping. The proposed design, disclosing the potential capability of producing higher power at one or two orders of magnitude than those commercially available on the market today, can dramatically reduce the development and installation (transportation) cost of an SSPS. For example, the total cost of a GW-class SSPS was estimated to be about 28,000M USD, and the total savings due to this improvement could be about 30% or USD 8400M. These attributes directly support microwave power transmission in space-based solar power by reducing hardware and implementation costs while extending service life. Therefore, continued development and prototyping of field-emission based rising-sun magnetrons for MPT are of considerable importance, which can help make SSPS a more viable and sustainable renewable energy source.

**Author Contributions:** Conceptualization, K.A. and M.-C.L.; methodology, K.A. and M.-C.L.; software, K.A. and M.-C.L.; validation, K.A. and M.-C.L.; formal analysis, K.A. and M.-C.L.; investigation, K.A. and M.-C.L.; resources, M.-C.L.; data curation, K.A. and M.-C.L.; writing—original draft preparation, K.A. and M.-C.L.; writing—review and editing, K.A. and M.-C.L.; visualization, K.A. and M.-C.L.; supervision, M.-C.L.; project administration, M.-C.L.; funding acquisition, M.-C.L. All authors have read and agreed to the published version of the manuscript.

**Funding:** This work was partially supported by the Hanyang University (No. HY-201400000002393), the National Research Foundation of Korea (No. 2015R1D1A1A01061017), and MASTEK, Inc. in Taiwan.

**Institutional Review Board Statement:** Not applicable.

**Informed Consent Statement:** Not applicable.

**Data Availability Statement:** The original contributions presented in this study are included in the article. Further inquiries can be directed to the corresponding author.

**Conflicts of Interest:** The authors declare that the research was conducted in the absence of any commercial or financial relationships that could be construed as a potential conflict of interest.

## References

1. Wood, D. *Space-Based Solar Power*; United States Department of Energy (DOE): Washington, DC, USA, 2014. Available online: https://www.energy.gov/articles/space-based-solar-power (accessed on 30 August 2025).
2. Glaser, P.E. Power from the sun: Its future. *Science* **1968**, *162*, 857–861. [CrossRef]
3. Glaser, P.E. Method and Apparatus for Converting Solar Radiation to Electrical Power. U.S. Patent US 3781647, 24 December 1973.
4. Glaser, P.E.; Maynard, O.E.; Mackovciak, J.J.R.; Ralph, E.I. *Feasibility Study of a Satellite Solar Power Station*; NASA CR-2357, ADL-C-74830; NASA Lewis Research Center: Cleveland, OH, USA, 1974. Available online: https://ntrs.nasa.gov/citations/19750015611 (accessed on 30 August 2025).
5. U.S. Department of Energy (DOE); NASA. *Satellite Power System Concept Development and Evaluation Program July 1977–August 1980*; DOE/ET-0034; U.S. Department of Energy (DOE): Washington, DC, USA, 1978. Available online: https://space.nss.org/satellite-power-system-concept-development-and-evaluation-program/ (accessed on 23 August 2025).
6. U.S. Department of Energy (DOE); NASA. *Satellite Power System Concept Development and Evaluation Program Reference System Report*; DOE/ER-0023; U.S. Department of Energy (DOE): Washington, DC, USA, 1978. Available online: https://space.nss.org/satellite-power-system-concept-development-and-evaluation-program/ (accessed on 23 August 2025).

7. Mankins, J.C. Testimony of John Mankins before House Science Committee Hearings on Solar Power Satellites. 2000. Available online: https://space.nss.org/testimony-of-john-mankins-before-house-science-committee-hearings-on-solar-power-satellites/ (accessed on 23 August 2025).
8. Dietz, R.H.; Arndt, G.D.; Seyl, J.W.; Leopold, L.; Kelley, J.S. *Satellite Power System: Concept Development and Evaluation Program: Volume 3, Power Transmission and Reception Technical Summary and Assessment*; Report No. S-507; U.S. Department of Energy (DOE); NASA: Washington, DC, USA, 1981. Available online: https://ntrs.nasa.gov/citations/19810019084 (accessed on 23 August 2025).
9. Mankins, J.C. A fresh look at space solar power: New architectures, concepts and technologies. *Acta Astronaut.* **1997**, *41*, 347–359. [CrossRef]
10. Worden, S.P. Dr. Pete Worden on the Space Show. 2009. Available online: https://www.thespaceshow.com/show/23-mar-2009/broadcast-1127-special-edition (accessed on 23 August 2025).
11. Cabinet Office, Government of Japan. Basic Plan for Space Policy. 2009. Available online: www8.cao.go.jp/space/english/index-e.html (accessed on 23 August 2025).
12. China Proposes Space Collaboration with India. 2012. Available online: https://timesofindia.indiatimes.com/india/china-proposes-space-collaboration-with-india/articleshow/17066537.cms (accessed on 23 August 2025).
13. Hou, X. Multi-Rotary Joints SPS – 2015 SunSat Design Competition. First Place Winner: China Academy of Space Technology (CAST). 2015. Available online: https://youtu.be/XhgJwnpYRGc?si=bbIKgoUwyjkneirW (accessed on 23 August 2025).
14. Hou, X.; Li, M.; Niu, L.; Zhou, L.; Chen, Y.; Cheng, Z.; Ji, H. SunSat Design Competition 2014–2015 First Place Winner–Team CAST: Multi-Rotary Joints SPS. *Online J. Space Commun.* **2021**, *11*, 4.
15. Tarantola, A. Scientists Make Strides in Beaming Solar Power from Space. 2015. Available online: https://www.engadget.com/2015-03-12-scientists-make-strides-in-beaming-solar-power-from-space.html (accessed on 23 August 2025).
16. Japan Space Scientists Make Wireless Energy Breakthrough. 2015. Available online: https://phys.org/news/2015-03-japan-space-scientists-wireless-energy.html (accessed on 23 August 2025).
17. Mitsubishi Heavy Industries, Ltd. MHI Successfully Completes Ground Demonstration Testing of Wireless Power Transmission Technology for SSPS. Press Information. 2015. Available online: https://www.mhi.com/news/1503121879.html (accessed on 23 August 2025).
18. Vaessen, P. Wireless power transmission. *Brief. Pap.* **2009**, *35*, 4.
19. Liu, M.; Liu, C.; Fuks, M.I.; Schamiloglu, E. Operation characteristics of 12-cavity relativistic magnetron with single-stepped cavities. *IEEE Trans. Plasma Sci.* **2014**, *42*, 3283–3287. [CrossRef]
20. Kim, H.J.; Shin, J.U.; Choi, J.J. Particle-in-cell code simulations on a rising-sun magnetron oscillator. *IEEE Trans. Plasma Sci.* **2002**, *30*, 956–961. [CrossRef]
21. Kim, J.-I.; Jeon, S.-G.; Jin, Y.-S.; Kim, G.-J.; Shon, C.-H. Three-dimensional particle-in-cell simulation of fast oscillation startup in strapped magnetron using electrically primed electrons. *Jpn. J. Appl. Phys.* **2007**, *46*, 6853. [CrossRef]
22. Kim, H.J.; Choi, J.J. Three-dimensional particle-in-cell simulation study of a frequency tunable relativistic magnetron. *IEEE Trans. Dielectr. Electr. Insul.* **2007**, *14*, 1045–1049. [CrossRef]
23. Lin, M.-C.; Nieter, C.; Stoltz, P.H.; Smithe, D.N. Accurately and efficiently studying the RF structures using a conformal finite-difference time-domain particle-in-cell method. *Open Plasma Phys. J.* **2010**, *3*, 48–52. [CrossRef]
24. Browning, J.; Fernandez-Gutierrez, S.; Lin, M.C.; Smithe, D.N.; Watrous, J. Phase control and fast start-up of a magnetron using modulation of an addressable faceted cathode. *Appl. Phys. Lett.* **2014**, *104*, 233507. [CrossRef]
25. Fernandez-Gutierrez, S.; Browning, J.; Lin, M.-C.; Smithe, D.N.; Watrous, J. Simulation of a rising sun magnetron employing a faceted cathode with a continuous current source. *J. Vac. Sci. Technol. B* **2014**, *32*, 061205. [CrossRef]
26. Fernandez-Gutierrez, S.; Browning, J.; Lin, M.-C.; Smithe, D.N.; Watrous, J. Phase-control of a rising sun magnetron using a modulated, addressable, current source. *J. Vac. Sci. Technol. B* **2015**, *33*, 031203. [CrossRef]
27. Fernandez-Gutierrez, S.; Browning, J.; Lin, M.-C.; Smithe, D.N.; Watrous, J. Dynamic phase-control of a rising sun magnetron using modulated and continuous current. *J. Appl. Phys.* **2016**, *119*, 044501. [CrossRef]
28. Guerrera, S.A.; Akinwande, A.I. Silicon field emitter arrays with current densities exceeding 100 A/cm$^2$ at gate voltages below 75 V. *IEEE Electron Device Lett.* **2016**, *37*, 96–99. [CrossRef]
29. Nieter, C.; Cary, J.R.; Werner, G.R.; Smithe, D.N.; Stoltz, P.H. Application of Dey–Mittra conformal boundary algorithm to 3D electromagnetic modeling. *J. Comput. Phys.* **2009**, *228*, 7902–7916. [CrossRef]
30. Nieter, C.; Cary, J.R. VORPAL: A versatile plasma simulation code. *J. Comput. Phys.* **2004**, *196*, 448–473. [CrossRef]
31. Saveliev, Y.M.; Kerr, B.A.; Harbour, M.I.; Douglas, S.C.; Sibbett, W. Operation of a relativistic rising-sun magnetron with cathodes of various diameters. *IEEE Trans. Plasma Sci.* **2002**, *30*, 938–946. [CrossRef]
32. Lau, Y.Y.; Luginsland, J.W.; Cartwright, K.L.; Simon, D.H.; Tang, W.; Hoff, B.W.; Gilgenbach, R.M. A re-examination of the Buneman–Hartree condition in a cylindrical smooth-bore relativistic magnetron. *Phys. Plasmas* **2010**, *17*, 033102. [CrossRef]
33. Andreev, A.D.; Hendricks, K.J. Metamaterial-like cathodes in multicavity magnetrons. *IEEE Trans. Plasma Sci.* **2012**, *40*, 2267–2273. [CrossRef]

34. Liu, M.; Huang, Z.; Fuks, M.I.; Jiang, W.; Schamiloglu, E.; Liu, C. Investigation of the operating characteristics of a 12-cavity rising-sun relativistic magnetron with diffraction output using particle-in-cell simulations. *Phys. Plasmas* **2016**, *23*, 052104. [CrossRef]
35. Liu, M.; Fuks, M.I.; Schamiloglu, E.; Liu, C. Frequency switching in a 12-cavity relativistic magnetron with axial extraction of radiation. *IEEE Trans. Plasma Sci.* **2012**, *40*, 1569–1574. [CrossRef]
36. Li, L.; Aranganadin, K.; Hsu, H.-Y.; Lin, M.-C. Design and development of field emission based magnetron for industrial applications using conformal finite-difference time-domain particle-in-cell simulations. *J. Vac. Sci. Technol. B* **2020**, *38*, 023205. [CrossRef]

**Disclaimer/Publisher's Note:** The statements, opinions and data contained in all publications are solely those of the individual author(s) and contributor(s) and not of MDPI and/or the editor(s). MDPI and/or the editor(s) disclaim responsibility for any injury to people or property resulting from any ideas, methods, instructions or products referred to in the content.